Design of Photovoltaic Microinverter for Off-Grid and Grid-Parallel Applications

Christian Felgemacher, Philipp Jäger, Ali Kobeissi, Jonas Pfeiffer, Dennis Wiegand,
Wolfram Kruschel, Benjamin Dombert, Samuel Vasconcelos Araújo, Peter Zacharias
University of Kassel
Centre of Competence for Distributed
Electric Power Technology (KDEE)
34121 Kassel, Germany

***Abstract*—The design and construction of a 500 VA microinverter for photovoltaic applications is presented. The developed microinverter is capable of operating as a standalone AC voltage source for small loads or, alternatively, as a grid-parallel system. Possible applications are therefore small off-grid installations as well as installations where space constraints do not allow enough modules to be combined to use string inverters. The design of the microinverter is based on a two stage concept. Two alternative topologies for the DC-DC converter stage have been considered. A prototype using a current-fed push-pull converter and a full-bridge output stage has been built and was shown to be operational. The prototype has achieved a maximum overall efficiency of 93.9 %, which includes all sensing, control and driving losses. SiC MOSFETs have been utilized to illustrate the capability of wide-band-gap devices.**

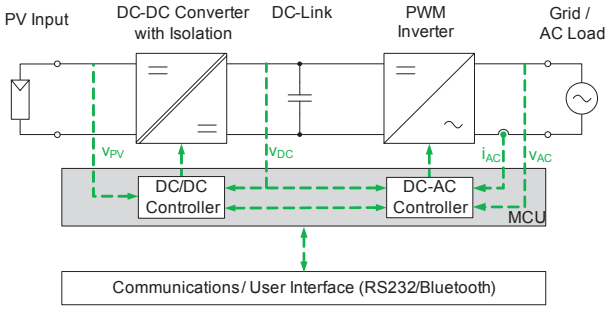

Fig. 1. System Level Block-Diagram

I. Introduction

In contrast to the more commonly used string inverters, which are connected to a number of photovoltaic modules connected in series, microinverters are typically connected only to a single module. There are certain benefits associated with the use of microinverters such as optimal tracking of the maximum power point (MPP) of each module, increased redundancy in case of inverter failure and ease of installation. However, there are also significant drawbacks. One of them is the low input voltage to the microinverter, which results in a requirement for a boost stage with a high voltage gain. Consequently, a two-stage design is often required, which reduces the overall efficiency. Additionally, specific costs of microinverters are generally higher than those of string inverters, due to the higher impact of overhead costs for control, driving, sensing and for safety functions; which in the case of a microinverter need to be implemented for each unit.

In some situations the benefits of microinverters may outweigh the drawbacks. Examples for such applications are small off-grid installations where only small AC loads need to be powered as well as small rooftop installations where modules can not be arranged in strings. This paper describes a design for a 500 VA microinverter. This power rating is larger that of typical microinverters and makes the device suitable to connect it to two photovoltaic modules. This is expected to reduce the specific cost of the device. The main aim in developing this design was to achieve a good overall efficiency at a relatively low cost for a microinverter system that is usable in grid-parallel as well as in off-grid applications. A further aim was to illustrate the potential of wide-band-gap semiconductors. The overall design specifications for the microinverter are summarized in Table I.

II. Selection of System Topology

The design of the microinverter is based on a two-stage concept as shown in figure 1. The main advantage of this approach is the decoupling of the constant input power flow and the pulsating output power flow by a high voltage DC link. A relatively large voltage ripple in the DC link can be tolerated if appropriate control techniques are utilized for the DC-DC controller to ensure that the 100/120 Hz ripple at the inverter input is minimized to avoid negative influences on the MPP tracking [1]–[3].

TABLE I
Microinverter Design Specifications

U_{in}	18 to 40 V
I_{in}	< 20 A
U_{out}	230 / 240 V_{RMS}
I_{out}	2.35 A_{RMS}
f_{out}	50 / 60 Hz
Output power factor	0.8 (leading or lagging)
Target efficiency	> 95 %

ISBN 978-3-8007-3578-5

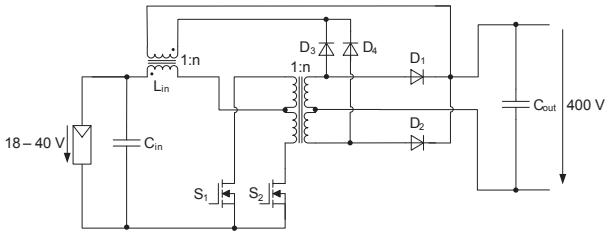

Fig. 2. Isolated Flyback-Current-Fed Push-Pull Converter

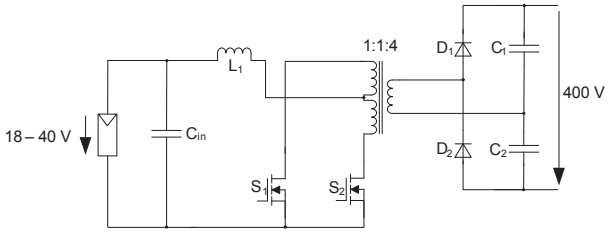

Fig. 3. Current-Fed Push-Pull Converter

A. Inverter Output Stage

One main design criteria for the converter is the ability to provide reactive power at the converter output up to a power factor of 0.8 leading or lagging. Designs using low frequency unfolder circuits in the output stage will not allow this criterion to be met. Therefore, only topologies that utilize high frequency switching to form the output waveform are considered for the output stage of the converter.

One option for the output stage is to use a half-bridge. This configuration has only two active switches and low driving effort. Only one semiconductor is in the conduction path at any time. However, a DC link voltage of larger than 700 V is required. Alternatively, a full-bridge stage can be used. This has the advantage of requiring a much lower DC link voltage of slightly more than 350 V at the disadvantage of always having two semiconductor devices in the current path, which results in increased conduction losses. The semiconductors can, however, have lower voltage ratings which should offset this disadvantage. It was decided to rely on a full-bridge topology for the DC-AC stage of the converter because of the ability to use the lower DC link voltage.

B. DC-DC Converter Stage

The DC-DC converter stage has to boost the PV input voltage (18 to 40 V) to a DC link voltage in excess of 350 V. Additionally, galvanic isolation between the input and output of the DC-DC stage is a desirable feature.

The isolated flyback-current-fed push-pull topology [4] shown in figure 2 as well as the current-fed push-pull topology shown in figure 3 were investigated.

Both considered topologies for the DC-DC stage provide galvanic isolation between the input and output and have the advantage of using only low-side switches, which reduces the driving effort that is required. The advantage of the topology shown in figure 2 is that it can be operated with duty cycles in the range from 0 to 0.5 (buck-mode) as well as in the range of 0.5 to 1 (boost mode) [4]. However, the output diodes have to block twice the output voltage, resulting in a required voltage rating of 1200 V for a DC link of 350 to 400 V.

The current-fed push-pull topology shown in figure 3 has the advantage that 600 V diodes can be used at the output. Additionally, the design of the transformer is easier, as no split output winding is required. The main disadvantage is that the converter can only operate with duty cycles above 0.5 (i.e. with overlapping MOSFET operation) and that the switches need to be protected if for some reason both MOSFETs are turned off, as in that case no current path exists for the current in the input inductor. This can be achieved using suppressor diodes in parallel to the MOSFETs or a snubber circuit.

Based on the presented comparison the current-fed push-pull topology was chosen for implementation in the microinverter. The smaller number of components and the lower voltage rating of the diodes were judged to outweigh the restriction of only operating in boost mode.

III. Prototype Design

This section describes the hardware design for the presented prototype. An overview of the power electronic topology of the developed microinverter is shown in figure 4. Details of the selection of the semiconductors as well as the design of the magnetic elements and the DC link are presented. Finally, a brief description of the sensing and control hardware as well as the auxiliary supplies is given.

A. Semiconductors

A total of six active switches and two diodes are used in the prototype. Each switch in the input stage of the microinverter has to block the voltage reflected across the transformer, which amounts to approximately 100 V. Additionally, overvoltages occur when the switches are turned off, as a consequence of the leakage inductance of the transformer. To protect the switches an RC snubber was added. Suppressor diodes have also been added to protect the switches against overvoltages which occur, if both devices are turned off and the energy stored in L_1 is discharged. In the prototype 200 V MOSFETs have been used to provide a large safety margin. To minimize losses 600 V SiC Schottky diodes have been used in the rectifier stage.

The devices in the fullbridge output stage of the microinverter require a voltage rating somewhat larger than the maximum voltage of the DC-link. Fast switching IGBTs with a maximum voltage rating of 600 V would be suitable for the application. Alternatively, it was considered to use 600 V GaN devices, which have significantly lower losses. As these devices were not available, 1200 V SiC MOSFETs were used for the prototype. While these are overrated in terms of their blocking voltage capability, they can illustrate the effects of reduced switching losses associated with wide-band-gap semiconductors.

ISBN 978-3-8007-3578-5

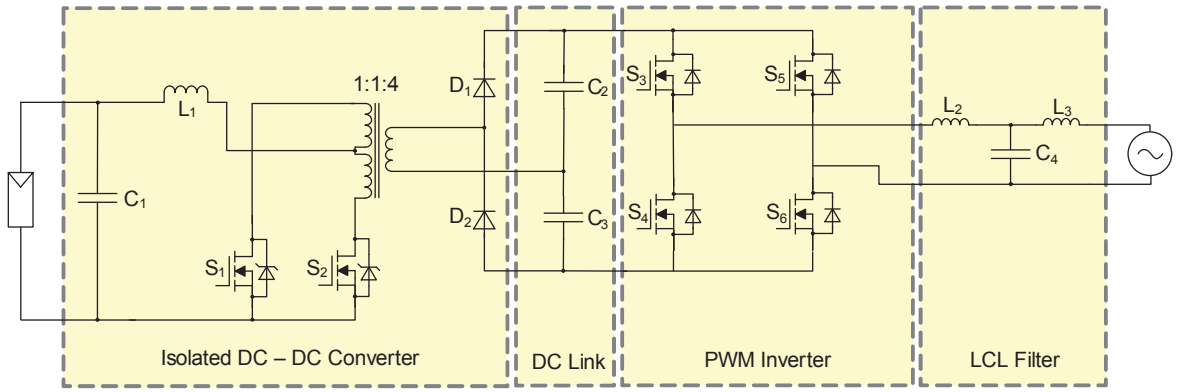

Fig. 4. Power Electronic Topology of Microinverter Prototype

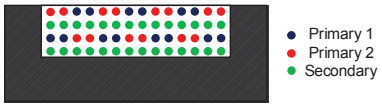

Fig. 5. Layout of Transformer Windings

B. Magnetic Elements

The microinverter contains three magnetic elements, the input inductor, the push-pull transformer and the output filter inductor. The input inductor is designed for an inductance of 30 μH and a maximum current of 20 A. The inductor was built using an ETD 39 core (Mf 106) and twelve turns using 600x0.1mm litz wire.

The transformer was designed for a turns ratio of 1:1:4 with two primary windings. Additionally, achieving a low leakage inductance was essential, as the energy stored in the leakage inductance is lost in each switching cycle and imposes stress on the suppressor diodes and the RC snubber circuit. To achieve a low leakage inductance the winding strategy illustrated in figure 5 was used. The transformer design parameters are provided in table II.

The output filter inductor is required to filter out the switching frequency components of the output current of the fullbridge inverter. An LCL filter combination was selected for the microinverter. The inverter side inductor was designed for an inductance of 6.8 mH and a maximum current of 2.35 A using an amorphous metal core (AMCC-4) and two parallel strands of solid copper wire. The filter capacitance has been selected as 1 μF and the grid side inductor has an inductance of 0.1 mH.

TABLE II
TRANSFORMER SPECIFICATIONS

Core	ETD 49 (3C90)
P_{max}	550 VA
Primary Winding	7 turns (2 parallel strands of 160x0.1mm litz wire)
Secondary Winding	28 turns (90x0.1mm litz wire)
Switching Frequency	100 kHz

C. DC-link design

The capacitance required to limit the voltage fluctuation in the DC-link to a certain value ΔU_d can be calculated using the following equation [5].

$$C_{DC} = \frac{P_{out}}{2\pi \cdot f_{grid} \cdot U_{DC}^2} \cdot \frac{U_d}{\Delta U_d} \quad (1)$$

To ensure a maximum voltage variation in the DC-link of 5 % with a nominal DC-link voltage of 400 V and a maximum output power of 500 VA at a frequency of 50 Hz, a DC-link capacity of approximately 200 μF is required. In the prototype a total DC-link capacitance of 220 μF was used. As previously discussed the DC-link capacitance can be reduced further if suitable control strategies are employed to maintain a constant input voltage regardless of the variations in the DC-link. This has been identified as an option for further improvements.

D. Sensing and Control Hardware

To enable control of the microinverter in island mode as well as grid-parallel operation a set of measurements have to be taken. The parameters that need to be measured include the output voltage, output current and DC link voltage as well as the input voltage. The output voltage and DC link voltage are sensed by the analogue to digital converter in the microcontroller using high-impedance networks and operational amplifiers. The output current is measured using a hall-effect current sensing IC and the input voltage is sensed using an external analogue to digital converter that is connected to the microcontroller via a digital isolation IC using the I^2C interface. To control the system a single 32-bit microcontroller of the TI C2000 family was used and a simple RS232 / Bluetooth interface was developed to aid development and to provide status information. Providing status information through a wireless communication link has the added advantage of not requiring direct access to the device as well as increasing the user safety as the communication link has inherent galvanic isolation. A possibility for further optimization of the system efficiency is the use of a microcontroller that has a lower power consumption.

ISBN 978-3-8007-3578-5

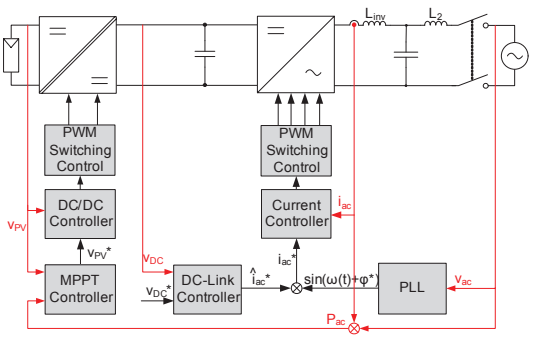

Fig. 6. Control Structure for Grid Parallel Operation

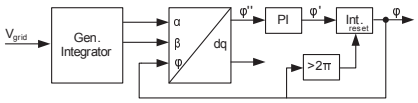

Fig. 7. Structure of PLL

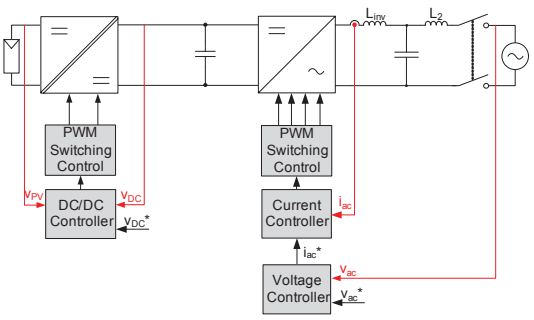

Fig. 8. Control Structure for Island Operation

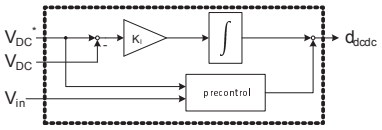

Fig. 9. Structure of DC link Voltage Controller

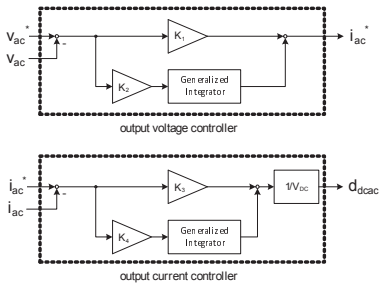

Fig. 10. Structure of Output Voltage and Current Controller

E. Auxiliary Supplies

All supplies for the gate drives as well as for the sensing and control subsystems are generated within the microinverter using commercial isolating DC-DC converters. While this is not a cost effective approach for a volume product it offers the ability to quickly build a compact system. To further improve the system, the development of a small and cost effective solution to supply the different components needs to be considered.

IV. Description of Control Strategy

Whereas the hardware that has been described in the previous section can be utilized to operate in grid-parallel as well as in island operation the control software needs to be adapted for each mode of operation. In this section the structure of a possible control system for each of the two modes of operation is presented. For the DC-AC stage a PWM scheme with unipolar voltage switching is used. This has the advantage of doubling the effective switching frequency in the output waveforms, leading to a reduction in the required filtering [6].

A. Grid-Parallel Operation

In grid-parallel operation the microinverter would be operated to extract the maximum power from the photovoltaic generator by means of maximum power point tracking. The DC-DC stage injects this current into the DC-link which is then injected into the grid by the output stage. The overall control structure for this mode of operation is shown in figure 6.

Details of the internal structure of the PLL are illustrated in figure 7. The PLL provides a reference signal in phase with the grid voltage. This signal is multiplied with the output current amplitude that is set by the DC link controller in order to maintain the DC link at 400 V and provided as the set-point to the current controller, which can be implemented as a proportional resonant controller [7].

The DC-DC controller adjusts the duty cycle for the DC-DC converter to maintain the input voltage at the value that is set by the maximum power point tracker. The maximum power point tracker in turn can use different algorithms [8], [9] to find the voltage at the maximum power point by varying the input voltage and observing changes in the output power of the microinverter. This approach eliminates the need for measuring the input current of the converter.

B. Island Mode Operation

In island mode the microinverter supplies a local load and is regulated to provide an output voltage of 230 / 240 V_{AC}, depending on the mode of operation. The power that the converter needs to provide is determined by the load. The DC-AC stage is controlled in order to provide the required output voltage, while the DC-DC converter is controlled to inject the power into the DC link that is required to maintain a constant DC link voltage. An overview of the control structure for island operation is provided in figure 8.

The voltage controller as well as the current controller in the control structure in figure 8 have been implemented as proportional resonant controllers and details of the two controller are shown in figure 10. The DC-DC controller consists of a feed-forward controller, which computes an expected duty-cycle that is require to maintain the DC link

ISBN 978-3-8007-3578-5

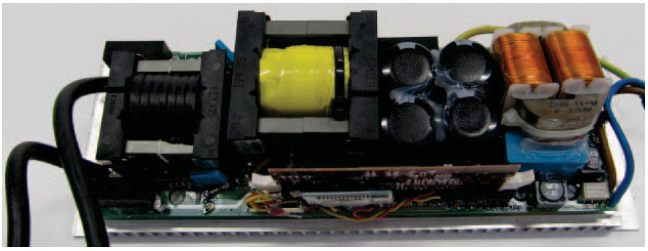

Fig. 11. Close up Photograph of Microinverter Prototype (Cover Removed)

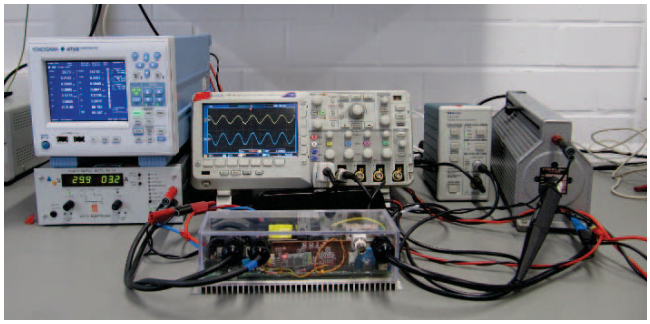

Fig. 12. Laboratory Setup of Microinverter, DC Source, Resistive Load and Measurement Equipment

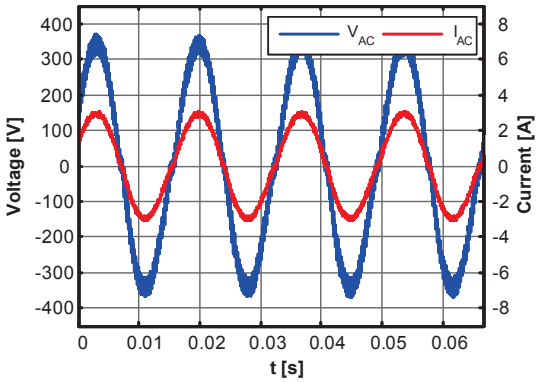

Fig. 13. Supplying a 500 W Resistive Load (60 Hz, 240 V_{rms}, $f_{sw,DCDC}$ = 30 kHz, $f_{sw,DCAC}$ = 8 kHz) - Measured Using Tektronix DPO2014

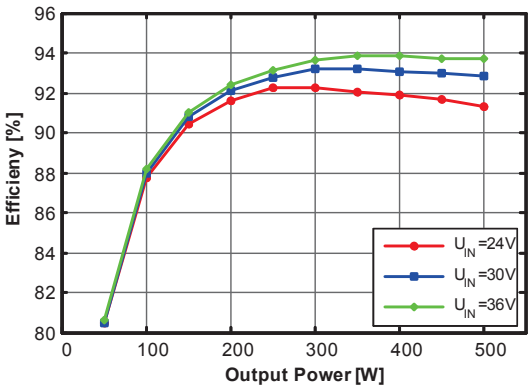

Fig. 15. Overall System Efficiency in Island Operation Measured Using Yokogawa WT500 (60 Hz, 240 V_{rms}, $f_{sw,DCDC}$ = 30 kHz, $f_{sw,DCAC}$ = 8 kHz)

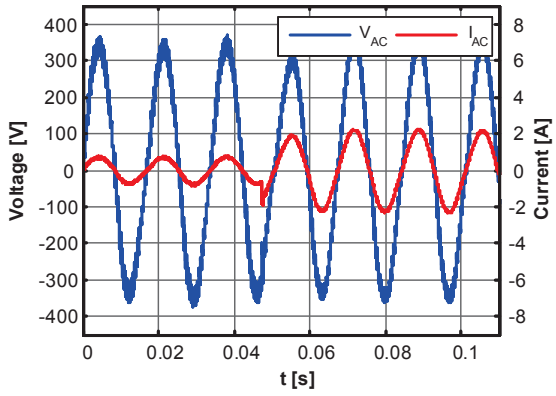

Fig. 14. Step Change in Output Load from 125 W to 375 W (60 Hz, 240 V_{rms}, $f_{sw,DCDC}$ = 30 kHz, $f_{sw,DCAC}$ = 8 kHz) - Measured Using Tektronix DPO2014

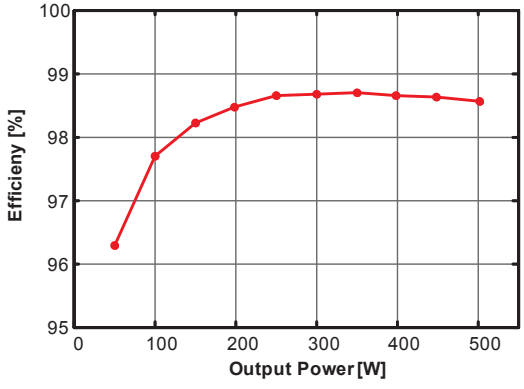

Fig. 16. Efficiency of DC-AC Stage Measured Using Yokogawa WT500 (60 Hz, 240 V_{rms}, $f_{sw,DCAC}$ = 8 kHz)

ISBN 978-3-8007-3578-5

TABLE III
LIST OF MAIN COMPONENTS

S_1,S_2	IPP110N20N3 3 (2 each)
D_1,D_2	C3D10060A
S_3,$S_4$$S_5$,$S_6$	C2M0080120D
C_1	6x 10 μF (ceramic)
C_2,C_3	2x 220 μF (electrolytic)
L_1,L_2,L_3,C_4	as described in previous sections
Snubbers on S_1 and S_2	2200 pF / 33 Ω

at 400 V based on the measured input voltage as well as an additional I-type controller, which is used to compensate the remaining error as shown in figure 9.

V. Experimental Results

A first prototype of the microinverter was constructed and is shown in figure 11. The prototype uses a single microcontroller and contains all the required sensing circuitry as well as auxiliary supplies. The power density of the standalone prototype is approximately 0.5 kW/dm^3. To demonstrate the capabilities of the prototype the control structure for island operation as described in the previous section has been implemented and some measurements were undertaken. The experimental setup is depicted in figure 12. The main components used in the prototype are those listed in table III.

In figure 13 the output current and voltage at the converter output are shown, while a resistive load of 500 W is connected. To illustrate the capability to react to changes in the load a step change from 125 W to 373 W is shown in figure 14.

The system efficiency was measured for different output powers and different input voltages. The measurements are shown in figure 15. A peak efficiency of 93.9 % was achieved at 400 W output power with an input voltage of 36 V. It should be noted that the efficiency measurements include the control and driving effort and all losses in the auxiliary supplies.

Further optimizations are necessary in order to reach the target efficiency of 95 %. To identify areas where improvements would be most beneficial the efficiency of the output stage alone has been measured. As can be seen from figure 16 the efficiency of the inverter stage using SiC MOSFETs is larger than 98.5 % for output powers in excess of 200 W. These results show that the main losses occur in the input stage of the microinverter. Further analysis has shown that the RC snubbers on the switches in the input stage contribute a large amount of the total losses. The focus of further optimizations of the design should therefore be on investigating how the design of the DC-DC converter and the transformer can be optimized in order to reduce these losses.

VI. Conclusion

A design for a 500 VA photovoltaic microinverter has been presented. Applications for such an inverter may be small off-grid installations where small AC loads need to be supplied as well as rooftop installations where modules can not be arranged in strings.

The developed system is based on a two stage concept. After comparing two possible DC-DC topologies for the input stage a prototype of the microinverter using a current-fed push-pull converter in combination with a fullbridge inverter stage has been built and was shown to be operational. The prototype uses a single microcontroller and contains all the required sensing as well as auxiliary supplies. A peak efficiency of 93.9 % was achieved. The system is suitable for different grid frequencies and nominal voltages and can also supply reactive power.

To improve the system efficiency the DC-DC stage needs to be further optimized. The use of wide-band-gap devices, particularly low-voltage GaN switches, may offer advantages. Additionally, the improvement of the transformer design and the use of more suitable 600 V GaN devices in the output stage of the inverter needs to be investigated.

References

[1] N. Femia, G. Petrone, G. Spagnuolo, and M. Vitelli, "A Technique for Improving P&O MPPT Performances of Double-Stage Grid-Connected Photovoltaic Systems," *Industrial Electronics, IEEE Transactions on*, vol. 56, no. 11, pp. 4473–4482, 2009.

[2] F. Shinjo, K. Wada, and T. Shimizu, "A Single-Phase Grid-Connected Inverter with a Power Decoupling Function," in *Power Electronics Specialists Conference, 2007. PESC 2007. IEEE*, 2007, pp. 1245–1249.

[3] E. Mamarelis, C. Ramos-Paja, G. Petrone, G. Spagnuolo, M. Vitelli, and R. Giral, "FPGA-based controller for mitigation of the 100 Hz oscillation in grid connected PV systems," in *Industrial Technology (ICIT), 2010 IEEE International Conference on*, 2010, pp. 925–930.

[4] G. V. Torrico Bascope and I. Barbi, "Isolated flyback-current-fed push-pull converter for power factor correction," in *Proc. th Annual IEEE Power Electronics Specialists Conf. PESC '96 Record*, vol. 2, 1996, pp. 1184–1190.

[5] P. Zacharias, Ed., *Use of Electronic-Based Power Conversion for Distributed and Renewable Energy Sources*. ISET, 2008.

[6] N. Mohan, T. M. Underland, and W. P. Robbins, *Power Electronics: Converters, Applications, and Design*, 3rd ed. John Wiley & Sons, Inc, 2003.

[7] R. Teodorescu, F. Blaabjerg, M. Liserre, and P. Loh, "Proportional-resonant controllers and filters for grid-connected voltage-source converters," *Electric Power Applications, IEE Proceedings* -, vol. 153, no. 5, pp. 750–762, 2006.

[8] M. de Brito, L. Galotto, L. Sampaio, G. de Azevedo e Melo, and C. Canesin, "Evaluation of the main mppt techniques for photovoltaic applications," *Industrial Electronics, IEEE Transactions on*, vol. 60, no. 3, pp. 1156–1167, 2013.

[9] D. Sera, T. Kerekes, R. Teodorescu, and F. Blaabjerg, "Improved mppt algorithms for rapidly changing environmental conditions," in *Power Electronics and Motion Control Conference, 2006. EPE-PEMC 2006. 12th International*, 2006, pp. 1614–1619.

ISBN 978-3-8007-3578-5